AD-A096 320 IOWA UNIV IOWA CITY DEPT OF PHYSICS AND ASTRONOMY F/G 20/14
THE KILOMETRIC RADIO EMISSION SPECTRUM: RELATIONSHIP TO AURORAL--ETC(U)
JAN 81 D A GURNETT, R R ANDERSON N00014-76-C-0016
UNCLASSIFIED U. OF IOWA-81-4 NL

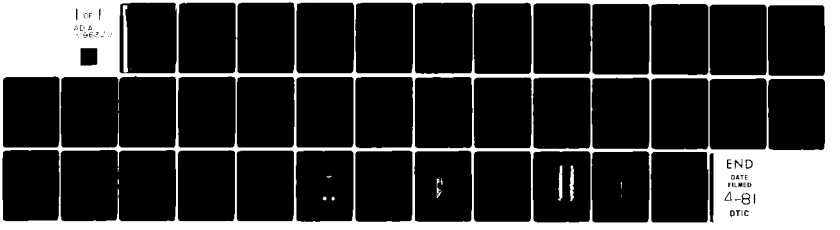

END
DATE FILMED
4-81
DTIC

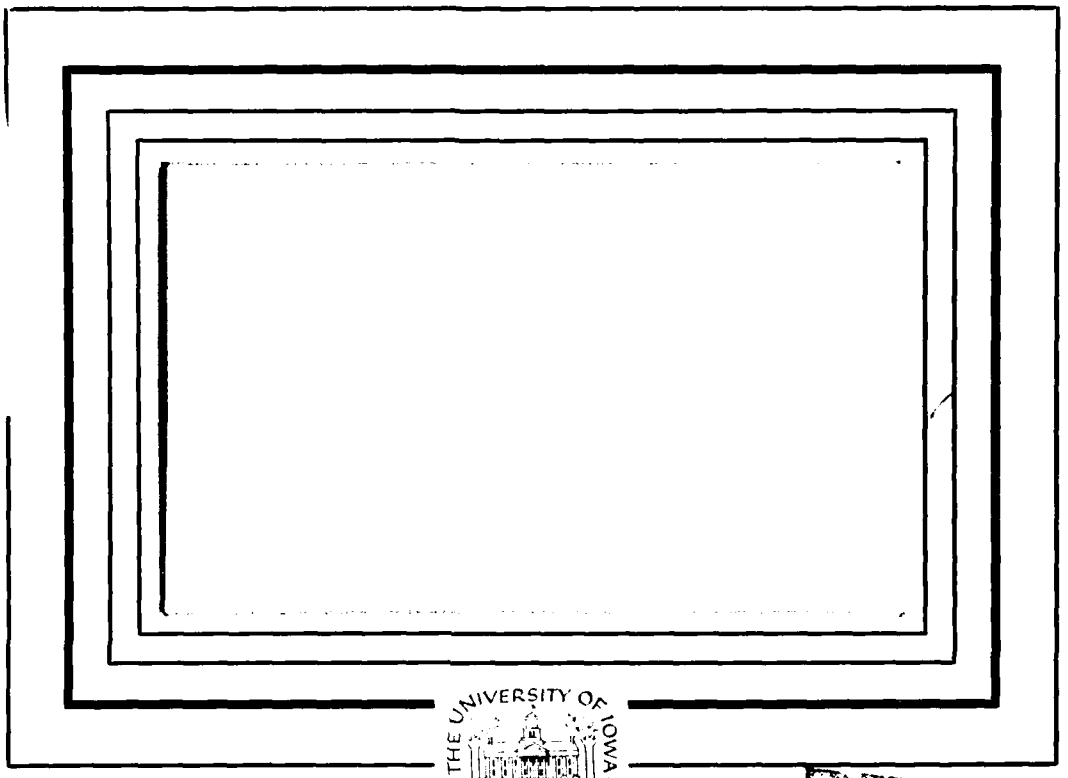

Department of Physics and Astronomy

THE UNIVERSITY OF IOWA

Iowa City, Iowa 52242

II

10

U. of Iowa 81-4

The Kilometric Radio Emission Spectrum: Relationship to Auroral Acceleration Processes+

by

D. A. Gurnett and R. R. Anderson

January 1981

Department of Physics and Astronomy
The University of Iowa
Iowa City, IA 52242

+Invited paper presented at the Chapman Conference on the Formation of Auroral Arcs, Fairbanks, Alaska, July 21, 1980.

The research presented in this paper was supported by NASA through Contract NAS5-20093 from Goddard Space Flight Center and by Grants NGL-16-001-043 and NGL-16-001-002 from NASA Headquarters, and by the Office of Naval Research.

UNCLASSIFIED

SECURITY CLASSIFICATION OF THIS PAGE (When Data Entered)

REPORT DOCUMENTATION PAGE		READ INSTRUCTIONS BEFORE COMPLETING FORM
1. REPORT NUMBER U. of Iowa 81-4	2. GOVT ACCESSION NO. AD-A097320	3. RECIPIENT'S CATALOG NUMBER
4. TITLE (and Subtitle) THE KILOMETRIC RADIO EMISSION SPECTRUM: RELATIONSHIP TO AURORAL ACCELERATION PROCESSES		5. TYPE OF REPORT & PERIOD COVERED Progress January 1981 6. PERFORMING ORG. REPORT NUMBER
7. AUTHOR(s) D. A. GURNETT and R. R. ANDERSON		8. CONTRACT OR GRANT NUMBER(s) N00014-76-C-0016
9. PERFORMING ORGANIZATION NAME AND ADDRESS Department of Physics and Astronomy The University of Iowa Iowa City, Iowa 52242		10. PROGRAM ELEMENT, PROJECT, TASK AREA & WORK UNIT NUMBERS
11. CONTROLLING OFFICE NAME AND ADDRESS Office of Naval Research Electronics Program Office Arlington, Virginia 22217		12. REPORT DATE 31 January 1981 13. NUMBER OF PAGES 36
14. MONITORING AGENCY NAME & ADDRESS(if different from Controlling Office)		15. SECURITY CLASS. (of this Report) UNCLASSIFIED 15a. DECLASSIFICATION/DOWNGRADING SCHEDULE

16. DISTRIBUTION STATEMENT (of this Report)

Approved for public release; distribution is unlimited

17. DISTRIBUTION STATEMENT (of the abstract entered in Block 20, if different from Report)

18. SUPPLEMENTARY NOTES

To be published in J. Geophys. Res., 1981

19. KEY WORDS (Continue on reverse side if necessary and identify by block number)

Kilometric Radio Emission
Auroral Acceleration Processes
Plasma Waves

20. ABSTRACT (Continue on reverse side if necessary and identify by block number)

(See page following)

DD FORM 1 JAN 73 1473 EDITION OF 1 NOV 65 IS OBSOLETE
S/N 0102-014-6601

UNCLASSIFIED
SECURITY CLASSIFICATION OF THIS PAGE (When Data Entered)

ABSTRACT

Satellite measurements have now confirmed that intense radio emissions called auroral kilometric radiation are generated at altitudes of 2 to 3 R_E over the auroral regions. These radio emissions are believed to be generated by Doppler-shifted cyclotron radiation from the electrons involved in the auroral acceleration process. Using current theories for the generation of this radiation we discuss the possibilities for obtaining information on the auroral acceleration processes from the spectrum of this radiation. For example, under certain conditions it is shown that the low frequency cutoff provides a direct indication of the upper altitude limit of the acceleration region. Also, certain drifting features in the spectrum can be interpreted in terms of the propagation of shock-like disturbances along the auroral field lines at velocities near the ion-acoustic speed.

I. INTRODUCTION

Spacecraft observations over the last decade have revealed that the earth is an intense radio source in the kilometer wavelength range and that the generation of this radiation is closely associated with the auroral acceleration process. The first reports of this radiation were by Benediktov et al. [1965] and Dunkel et al. [1970] who identified intense radio emissions which were closely correlated with high latitude magnetic disturbances. Later studies by Gurnett [1974] showed that the peak intensity occurred at kilometer wavelengths and that the radio emissions were generated at low altitudes over the auroral regions in association with discrete auroral arcs. During bright auroral displays the maximum power radiated was found to be very large, $\sim 10^9$ watts. The earth is, therefore, a very intense radio emitter, comparable in many respects to Jupiter, which has long been recognized as an intense planetary radio source. Because of the association with discrete auroral arcs, Gurnett [1974] suggested that the radiation was associated with the inverted-V electron precipitation bands detected by low-altitude satellites [Frank and Ackerson, 1971]. This relationship has now been confirmed by direct in situ measurements in the auroral regions [Bensen and Calvert, 1979; Green et al., 1979]. Polarization measurements by Gurnett and Green [1978] and Kaiser et al. [1978] showed that kilometric radiation is generated in the right-hand extraordinary mode. Of the many theories which have been proposed, the observed polarization and the

absence of intense electrostatic waves in the source region have greatly restricted the possible generation mechanisms. The most promising mechanisms at the present time appear to be the direct electromagnetic instabilities proposed by Melrose [1976] and Wu and Lee [1979].

In this paper we consider the relationship of the auroral kilometric radiation spectrum to the spatial structure and processes occurring in the auroral acceleration region. The basic objective is to explore the possibilities of using the emission spectrum to provide information about the details of the acceleration process. The methods employed may also have much broader applications. It now appears that the radio emission mechanism operative in the terrestrial auroral regions is a universal process occurring in association with the formation of auroral arcs throughout the solar system. For example, at both Jupiter and Saturn the same basic radio emission process is believed to be associated with auroral arcs occurring at these planets [Warwick et al., 1979; Kaiser, 1980]. Furthermore, radio emissions of the same type have also been tentatively identified from the planet Uranus [Brown, 1976]. Since it will not be possible to conduct direct in situ measurements of aurora at any of these planets in the near future, any advances which can be made in understanding the relationship of the radio emission spectrum to the auroral acceleration may provide a valuable tool for studying auroral acceleration processes in other regions of the solar system.

II. UPPER AND LOWER CUTOFF FREQUENCIES

A basic characteristic of the kilometric radio emission is the existence of well-defined upper and lower cutoff frequencies. Figure 1, for example, shows a typical auroral kilometric radiation event observed by the ISEE 1 spacecraft in the local evening region of the magnetosphere. As can be seen the radio emission spectrum has clearly identified upper and lower cutoffs which fluctuate over a wide range on a time scale of ten minutes or less. Except for fine structure, which will be discussed later, the radio emission normally extends continuously over the entire frequency band between the upper and lower cutoffs. Occasionally the radiation disappears for short periods, for example, from about 0145 to 0210 UT and from about 1000 to 1630 UT in Figure 1. The termination of the radiation often appears to result from a decrease in the bandwidth, with the upper and lower cutoffs merging as the radiation disappears.

If the radio emission is generated by Doppler-shifted cyclotron radiation, as in the models of Melrose [1976] and Wu and Lee [1979], a simple explanation can be advanced for the upper and lower cutoff frequencies. Before discussing the origin of these cutoffs, it is useful to first review the essential features of the cyclotron resonance mechanism. From very general considerations the growth rate for the right-hand extraordinary mode can be written

$$\omega_i = \frac{\pi c^2 \omega_p^2}{4\omega_g} \frac{N_H}{N_e} \int_C dv_\parallel v_\perp \left[\frac{\partial F}{\partial v_\perp} + n\cos\theta \frac{\omega}{\omega_g} \frac{v_\perp}{c} \frac{\partial F}{\partial v_\parallel} \right] \qquad (1)$$

where N_H and N_C are the hot and cold electron densities, ω_p and ω_g are the electron plasma frequency and gyrofrequencies, and $v_\parallel$ and $v_\perp$ are the parallel and perpendicular velocities relative to the magnetic field. The integral must be evaluated over a contour C in velocity space defined by the cyclotron resonance condition,

$$\omega - \omega_g \sqrt{1 - \frac{v_\perp^2 + v_\parallel^2}{c^2}} - v_\parallel \frac{\omega n}{c} \cos\theta = 0 \quad , \tag{2}$$

where n is the index of refraction, θ is the wave normal angle with respect to the magnetic field and ω is the wave frequency. As pointed out by Wu and Lee [1979], it is important to keep the relativistic term in Equation 2 even for velocities much less than the speed of light.

Two free-energy sources can be identified in Equation 1, one corresponding to regions of positive $\partial F/\partial v_\perp$ and the other corresponding to regions of positive $\partial F/\partial v_\parallel$. The condition $\partial F/\partial v_\perp > 0$ is characteristic of a loss-cone distribution function, and $\partial F/\partial v_\parallel > 0$ is characteristic of a beam-type distribution. A loss-cone distribution was the basis of Wu and Lee's [1979] theory of auroral kilometric radiation and a beam-type distribution was the basis of Melrose's [1976] theory. These two types of distribution functions are illustrated in Figure 2. In both cases the presence of a field-aligned electrostatic potential gradient plays a crucial role in establishing the essential features of the distribution function. As discussed by Chiu and Schulz [1978], in the presence of a parallel electric field the velocity distribution is divided into five regions by a loss-cone boundary, shown by the solid hyperbola-shaped lines in Figure 2, and an electrostatic acceleration boundary, shown by the dashed elliptical curve. The hyperbola-shaped loss cone arises because of

the acceleration caused by the parallel electric field between the spacecraft and the atmosphere. The elliptical electrostatic acceleration boundary represents the boundary for magnetospheric electrons accelerated by parallel electric fields above the spacecraft. The shaded region bounded by the hyperbola and the ellipse consists of particles trapped in the potential well formed by the mirror force below the satellite and the electrostatic potential barrier above the satellite. For the loss-cone instability it is sufficient for the moment to point out that a large $\partial F/\partial v_\perp$ is expected along the loss-cone boundary. In the case of the beam-type instability a large $\partial F/\partial v_\parallel$ arises because of the acceleration of low energy magnetospheric electrons by parallel electric fields above the spacecraft.

Inspection of distribution functions measured at various points along the auroral field lines shows evidence of both the beam and loss-cone free-energy sources. Figure 3, for example, shows a typical electron velocity distribution function from S3-3 [Mizera and Fennell, 1977] which has regions of large $\partial F/\partial v_\parallel$ and $\partial F/\partial v_\perp$. The region of large $\partial F/\partial v_\parallel$ occurs for downward moving electrons just inside the elliptical electron acceleration boundary (dashed line) and inside the loss cone. The distribution function in this region is somewhat different than the bimaxwellian used by Melrose for the electrostatically accelerated electron beam, but the basic free-energy source is the same. The region of large $\partial F/\partial v_\parallel$ occurs at a velocity of approximately $v_\parallel = \sqrt{2e\Phi_s/m}$, where Φ_s is the electrostatic potential at the spacecraft measured with respect to the potential above the acceleration region. The large parallel velocity gradient in this region arises because of the markedly decreased particle population

inside the electrostatic acceleration and loss-cone boundaries. This region of velocity space is only accessible to electrons from the ionosphere, which have much lower energies and therefore much lower phase-space densities than the magnetospheric electrons. As can be seen in Figure 3, the region of large $\partial F/\partial v_\perp$ occurs for upward moving electrons just inside the loss-cone boundary. The perpendicular velocity gradients are particularly large near and inside the elliptical electron acceleration boundary, at parallel velocities $v_\parallel \lesssim \sqrt{2e\Phi_s/m}$. Examination of other distribution functions shows that this relationship appears to be a consistent feature of the S3-3 observations. The $v_\parallel \lesssim \sqrt{2e\Phi_s/m}$ constraint on the region of large $\partial F/\partial v_\perp$ apparently arises because of the increased electron intensities in the loss cone at higher energies, probably due to backscattered beam electrons, which tend to have velocities greater than $\sqrt{2e\Phi_s/m}$. At the present time it is not known which of the two free-energy sources is most important. A decision on this question awaits a detailed evaluation of the growth rate from Equation 1 using the measured distribution function. Simple considerations, however, suggest that the loss-cone source is probably more important because the factors $v_\perp/c$ and CosΘ strongly reduce the contribution due to $\partial F/\partial v_\parallel$ in Equation 1.

Having discussed the essential features of the electron distribution function required for instability we can now discuss the physical reasons for upper and lower cutoffs in the radio emission spectrum. In order to have an instability it is essential that the cyclotron resonance velocity given by Equation 2 be at sufficiently low velocities to

be in the region of the distribution function where the velocity gradients are large. At low velocities, $v << c$, and for an index of refraction $n \simeq 1$, Wu and Lee [1979] have shown that the cyclotron resonance condition is a circle in the $v_\parallel$, $v_\perp$ plane with a center at $v_\parallel = c\mathrm{Cos}\theta$ and a radius of $v_R = c[\mathrm{Cos}\theta - 2\Delta\omega/\omega_g)]^{1/2}$, where $\Delta\omega = \omega - \omega_g$. A representative resonance circle is shown in Figure 2. Instability occurs when ω and θ are such that the resonance circle passes through a sufficiently large region of positive $\partial F/\partial v_\parallel$ or $\partial F/\partial v_\perp$, thereby giving a positive value for the integral in Equation 1. It is evident that a low resonance velocity implies propagation angles close to $\pi/2$ and wave frequencies close to the electron gyrofrequency. From Equation 2 one can show that the minimum resonance velocity occurs at $v_{\parallel Res}(\mathrm{Min}) = c(\Delta\omega/\omega)$. The minimum resonance velocity is therefore a very sensitive function of the wave frequency, decreasing rapidly as ω approaches ω_g. The wave frequency, however, is constrained to be above the extraordinary mode cutoff which occurs at

$$\omega_{R=0} = \frac{\omega_g}{2} + \sqrt{\left(\frac{\omega_g}{2}\right)^2 + \omega_p^2} \quad . \tag{3}$$

The minimum resonance energy is then approximately

$$W_{\parallel RES}(\mathrm{Min}) = \frac{1}{2} m c^2 \left(\frac{\Delta\omega_{R=0}}{\omega_g}\right)^2 \tag{4}$$

where $\Delta\omega_{R=0} = \omega_{R=0} - \omega_g = -\omega_g/2 + \sqrt{(\omega_g/2)^2 + \omega_p^2}$.

The variation of the minimum resonance energy with radial distance along an auroral field line is illustrated in Figure 4. As can be seen from Equation 3 the extraordinary mode cutoff, $\omega_{R=0}$, tends to be at either

ω_p or ω_g, which ever is larger. When $\omega_p > \omega_g$ the resonant energies are very large because a very large velocity is required to Doppler shift the emission frequency above the extraordinary mode cutoff. As ω_p decreases below ω_g, the minimum resonance energy decreases rapidly, to approximately $W_{\parallel Res}(Min) \simeq (1/2)mc^2(\omega_p/\omega_g)^4$ when $\omega_p << \omega_g$. As shown in Figure 4 the condition $\omega_p < \omega_g$ tends to occur at intermediate altitudes between the ionosphere and the outer magnetosphere. If the resonance energy drops below the characteristic energy $e\Phi_s$ of the free-energy source in the electron distribution (where the velocity gradients are large) then instability can occur. For a given electrostatic potential distribution along the field line this condition implies upper and lower boundaries for the unstable region, for example, A-A′ and B-B′ in Figure 4. These boundaries in turn imply upper and lower cutoffs for the radio emission spectrum. In practice, of course, these boundaries are not as precisely defined as indicated in Figure 4 because the growth rate given by Equation 1 involves an integral over the resonance velocity. This model does, however, provide us with a qualitative guide to analyze how the bandwidth of the emitted radiation depends on the parameters of the system.

We now return to the interpretation of the observed cutoffs of the auroral kilometric radiation. It is evident from Figure 4 that two basic factors control the bandwidth of the emitted radiation: (1) the plasma density distribution via the dependence of $W_{\parallel Res}(Min)$ on ω_p/ω_g, and (2) the detailed profile of the electrostatic potential distribution Φ_s. Two extreme situations can be identified. If the main electron acceleration occurs at very high altitudes, as in case B-B′, then the bandwidth is controlled almost completely by the points where the plasma frequency profile crosses the electron gyrofrequency profile. In this case, the

cutoff frequencies are almost completely determined by the plasma density distribution. On the other hand if the main electron acceleration occurs at lower altitudes, as in case A-A', then the lower cutoff frequency is controlled by the electron gyrofrequency at the upper boundary of the acceleration region. The upper cutoff is determined by a combination of factors. If the potential intersects on the steep part of the $W_{\parallel \mathrm{Res}}$ curve then the upper cutoff is essentially determined by the plasma density profile at the point where $\omega_p = \omega_g$. If the potential is lower then the upper cutoff frequency depends on the details of the potential profile, tending to decrease as Φ_s decreases.

Not much is known about the variability of the plasma density profile at high altitudes. The main information comes from the S3-3 satellite at about 2.0 R_E and various eccentric orbiting spacecraft at somewhat greater radial distances. Present indications are that $\omega_p \ll \omega_g$ at 2.0 R_E (R. Torbert, personal communication), more or less in agreement with the model in Figure 4. At larger radial distances, > 5 R_E, the plasma density is quite low, $N_e < 10$ cm^{-3}, which implies that the plasma frequency profile probably stays below the electron gyrofrequency out to about 5 R_E, as in Figure 4. Since the low frequency cutoff of the kilometric radiation usually corresponds to radial distances less than 5 R_E, it is tempting to assume that variations in the low frequency cutoff are caused by variations in the upper altitude limit of the acceleration region, as in case A-A' of Figure 4. Unfortunately, so little is known about the density distribution along the auroral field lines one cannot be certain whether this assumption is valid or not. If it is, then the low frequency cutoff gives a direct indication of the upper altitude limit of the acceleration region.

A probability distribution for the upper and lower cutoff frequencies obtained from a portion of the event in Figure 1 is shown in Figure 5. A radial distance scale derived from the electron gyrofrequency, which is always very close to the emission frequency, is shown at the bottom of this illustration. If the plasma frequency remains sufficiently low at high altitudes, as in case A-A', these low frequency cutoffs imply an upper limit to the electron acceleration region of about 2.0 to 3.5 R_E. Alternatively, these low frequency cutoffs may be representative of the radial distance at which the plasma frequency crosses the gyrofrequency, as in case B-B'. The interpretation of the high frequency cutoff is more certain. At frequencies above 300 kHz the high frequency cutoff is almost certainly controlled by the crossover between the plasma frequency and gyrofrequency profiles which occurs at about 1.5 R_E. At lower frequencies this cutoff becomes more dependent on the electrostatic potential near the crossover point, with a decreasing upper cutoff frequency indicating a smaller accelerating potential.

As discussed earlier, the radiation sometimes disappears completely during certain periods. At the beginning and end of these periods, the upper and lower cutoffs appear to merge as though the bandwidth of the emission decreased to zero at these points. Again two extreme interpretations are possible. The termination and onset of the emission could be due to changes in the plasma density profile or to changes in the electrostatic potential distribution. If changes in the plasma density are the controlling effect then the emissions would terminate completely as soon as the plasma frequency exceeds the gyrofrequency at all points along the magnetic field line. If such a density control does occur it seems almost certain that it would be imposed by density variations at

high altitudes rather than by variations in the ionosphere. Since rather high densities, $> 10^2 cm^{-3}$, would be required in the outer magnetosphere to completely quench the instability, it seems unlikely that changes in the density profile could play the dominant role in switching the radiation on and off. Temporal variations in the accelerating potential appear to be a more likely alternative. This viewpoint is supported by the fact that the kilometric radiation tends to disappear during periods of low magnetic activity [Voots et al., 1977] when field-aligned currents and the accelerating potential are expected to be the smallest. As can be seen from Figure 4, the basic model predicts that the upper and lower cutoffs, A and A', approach each other as the accelerating potential decreases, thereby shrinking the bandwidth to zero at the termination and onset of the emission, as is observed.

III. FINE STRUCTURE

Recently wideband measurements from the ISEE 1 and 2 spacecraft have provided very high resolution spectrum measurements of auroral kilometric radiation [Gurnett et al., 1979]. The spectrums obtained are remarkable because they show that the radiation consists of many discrete narrowband emissions, rather than a continuous broadband emission as suggested by the lower resolution measurements in Figures 1. Two representative high-resolution frequency-time spectrograms of auroral kilometric radiation are shown in Figure 6. These spectrograms cover a frequency range of 40 kHz, from 125 to 165 kHz, and a time interval of about 20 minutes. As can be seen, the spectrum is extremely complex. The most striking characteristic is the occurrence of many narrowband emissions with a bandwidth of 1 kHz or less. The entire auroral kilometric radiation spectrum appears to be made up of many discrete narrowband tones. Often the center frequency of the individual emissions varies in a systematic manner, sweeping either upward or downward across the spectrum. The spectrum in Figure 6, for example, is dominated by emissions drifting upward in frequency with increasing time. Comparable spectrums can also be found in which the emissions are sweeping downward in frequency. Careful examination shows that the drifting features are not always continuous tones, but sometimes consist of short bursts occurring on time scales of only a few seconds.

A contrasting example in which the drifting features are nearly absent is illustrated in Figure 7, which shows a 40-kHz frequency range, from 62.5 to 102.5 kHz, for two successive 1-minute intervals. The

spectrum in this case consists of a very large number of brief narrowband bursts. The duration and frequency range of the individual bursts is very small, typically 1 sec duration and 3 kHz frequency range, or less. The spectral shapes of the individual bursts vary over a wide range, sometimes sweeping upwards or downwards in frequency and forming various curved features on the frequency-time diagram.

The extremely complex spectral structure of the auroral kilometric radiation presents some difficult interpretational questions. The occurrence of many discrete narrowband emissions, as in Figure 7, is strongly reminiscent of chorus and other types of discrete whistler-mode emissions observed in the earth's magnetosphere [Helliwell, 1965]. The close similarity of the dynamic spectral characteristics may be more than purely coincidental, since both the auroral kilometric and whistler-mode instability mechanisms may be of essentially the same type. If the kilometric radiation is produced by a loss cone distribution then both instabilities involve a cyclotron resonance interaction with an anisotropic electron distribution. The detailed resonance condition and index of refraction are, of course, quite different, but otherwise the physical process is quite similar. For whistler-mode emissions it is generally agreed that the dynamic evolution of the spectrum is a highly nonlinear process involving electrons trapped by the rotating wave field [Inan et al., 1978]. It is possible that similar processes may be able to account for the discrete structure of the auroral kilometric radiation. It is interesting to note that if the generation of auroral kilometric radiation is essentially similar to the whistler-mode instability, then the kilometric radiation may play a significant role in the pitch-angle scattering of auroral electrons, similar to the pitch-angle scattering of

radiation belt electrons by whistler-mode emissions in the inner regions of the magnetosphere. Because the auroral kilometric radiation is generated in the right-hand polarized extraordinary mode the radiation carries away right-hand angular momentum, thereby reducing the pitch angle of the interacting electrons, very similar to the situation with whistler-mode interactions. Because the radiation intensities in the source are undoubtedly very large (10 to 100 mVm^{-1}), the pitch-angle diffusion rates could be a very significant factor in controlling the equilibrium electron velocity distribution in the auroral acceleration region. If such scattering occurs it should be characterized by time scales comparable to the time scale of the individual bursts, which is only a few seconds. Rapid fluctuations in inverted-V electron precipitation fluxes have been reported by various investigators, including for example Lin and Hoffman [1979], which could possibly be related to the fine structure of the kilometric radiation.

Probably the most important single feature which must be explained in the fine structure of the auroral kilometric radiation is the organization of the discrete bursts into upward and downward drifting bands of the type illustrated in Figure 6. The occurrence of quasi-monochromatic emissions sweeping through a large range of frequencies is a common feature of solar radio bursts [Kundu, 1965] and Jovian decametric radio emissions [Warwick, 1967]. These drifting features are usually interpreted as being due to the motion of the emitting particles, or a propagating disturbance, through a plasma which has a spatial gradient in the characteristic emission frequency. This model is used, for example, to explain the characteristic frequency drifts of type III and type IV solar radio bursts. In the case of the auroral kilometric radiation the

characteristic emission frequency is the electron gyrofrequency. Since the resonance energy is very sensitive to the frequency difference, $\Delta\omega$, between the emission frequency and the electron gyrofrequency, it is difficult to see how one can account for the large frequency range of the drifting emissions without involving a motion of the source.

Given that the emission takes place near the gyrofrequency, it is relatively easy to estimate the radial component of the source velocity, dR/dt, from the observed frequency drift rate, df/dt. For motion along a dipole field line at high latitudes, the velocity of the source is approximately

$$\frac{dR}{dt} = -\frac{R_E}{3}\left(\frac{f_{go}^{1/3}}{f^{4/3}}\right)\left(\frac{df}{dt}\right) \tag{5}$$

where $f_{go} \simeq 1.7$ MHz is the electron gyrofrequency at the surface of the earth in the auroral region. Using this equation we have estimated the source velocity using a random sample of the drifting emissions observed in the frequency range from 125 to 500 kHz. The distribution of source velocities is illustrated in Figure 8. As can be seen, the source velocities vary over a large range, from about 3 to 300 km/sec, with a median value of about 30 km/sec. Downward source motions are much more common than upward source motions.

To aid in the interpretation of these apparent source velocities corresponding electron and proton energy scales are shown at the top of Figure 8. As can be seen, the observed source velocities are much smaller than the typical electron and proton energies, 100 eV to 10 keV, observed along the auroral field lines. The observed drift rates cannot, therefore, be identified with the actual velocities of the auroral particles. In

considering other characteristic velocities which could be involved, two possibilities immediately come to mind: the Alfvén speed, $V_A = B/\sqrt{\mu_o \rho_m}$, and the ion-acoustic speed, $V_C = \sqrt{kT_e/m_i}$. Because the plasma density is quite low in the resonance interaction region ($\omega_p < \omega_g$) the Alfvén speed is too large, $V_A \gtrsim 2 \times 10^3$ km/sec, to be considered. The ion-acoustic speed is mainly determined by the electron temperature, T_e, and the ion mass, m_i. Using a temperature of 10^4 °K and assuming that O^+ is the dominant ion species, the ion-acoustic speed in the ionosphere is estimated to be about $V_C \simeq 2.3$ km/sec. For H^+ the ion-acoustic speed is about $V_c = 9.2$ km/sec. At higher altitudes the ion-acoustic speed tends to increase. An upper limit is given by the ion-acoustic speed in the plasma sheet, which is approximately $V_C \simeq 200$ km/sec. This range of ion-acoustic speeds is indicated in Figure 8. As can be seen, the observed source velocities are in approximately the same range as the estimated ion-acoustic speeds. This agreement suggests that the drifting tones observed in the auroral kilometric radiation may be caused by shock-like disturbances propagating along the auroral field lines at the ion-acoustic speed. The shock-like character of the disturbance is indicated by the narrow bandwidth of the drifting emissions, which suggests a spatial scale for the disturbance of about $\Delta R \simeq 50$ km. This mechanism would then be somewhat similar to the generation of type IV solar radio bursts which are produced by shock waves propagating through the solar corona [Kundu, 1965]. It has long been suspected from computer simulations [Hubbard and Joyce, 1979] and laboratory experiments [Carlqvist and Bostrom, 1970] that electrostatic structures in the auroral acceleration region may be highly turbulent, possibly consisting of many short duration transient disturbances propagating at speeds near the ion-acoustic speed. The exact mechanism by which these disturbances could

control the spectrum of the auroral kilometric radiation is not known, although numerous possibilities exist. If the potential perturbations are sufficiently large, then the disturbances may significantly modify the local electron velocity distribution, either by changing the loss-cone boundary, via the dependence on Φ_s, or by changing the reflection condition for the electrostatically trapped electron distribution. The changes could in turn affect the growth rate and spectrum of the radio emission, thereby producing drifting spectral features which appear to move with the disturbance.

IV. CONCLUSION

In this paper we have discussed the principal features of the spectrum of auroral kilometric radiation. Using current theories we have tried to relate these features to processes occurring in the auroral acceleration region. At the present time, it appears that the upper and lower cutoff frequencies of the auroral kilometric radiation can be readily understood if the radiation is produced by a Doppler-shifted cyclotron emission driven by either a loss-cone or beam distribution. The interpretation of the detailed variations of the upper and lower frequency cutoffs is complicated by uncertainties about the relative importance of variations in the plasma density profile and variations in the electrostatic potential distribution along the auroral field lines. If the electron plasma frequency is sufficiently low, $\lesssim$ 20 kHz, at high altitudes in the magnetosphere, then the lower frequency cutoff of the radio emission spectrum gives the upper limit to the auroral acceleration region. Typically, the upper limit of the acceleration region is located at radial distances from about 2.0 to 3.5 R_E. During some intervals the kilometric radiation completely disappears. These intervals are believed to correspond to either periods when the plasma density is unusually high, $\omega_p \gtrsim \omega_g$ at all points along the auroral field lines, or (more likely) to periods of very small accelerating potential.

High resolution frequency-time spectrums of auroral kilometric radiation show that the radiation consists of many discrete narrowband emissions, some of which drift upwards or downwards over a large frequency range. The existence of this very complex fine structure indicates the presence of corresponding complex spatial and temporal structure in the auroral acceleration region. The drifting narrowband emissions indicate the presence of very compact source regions, with radial scale sizes of only 50 km, which move upward or downward along the magnetic field line with velocities ranging from 3 to 300 km/sec. These source velocities are comparable to the ion-acoustic speed in the auroral ionosphere, which suggests the existence of shock-like disturbances propagating along the auroral field lines. These disturbances may possibly originate from unstable fluctuations in the electrostatic potential distribution, possibly forming transient double-layers or shock-like structures propagating along the magnetic field line. The fine structure of the auroral kilometric radiation also has features which are remarkably similar to discrete whistler-mode emissions, suggesting that somewhat similar nonlinear processes may be involved in both types of radio emissions.

ACKNOWLEDGEMENTS

The authors would like to express their thanks to Y. Chiu, J. Fennell and D. Croley of the Aerospace Space Science Laboratory for several useful discussions concerning the S3-3 electron distribution functions and possible relationships to auroral kilometric radiation.

The research presented in this paper was supported by NASA through Contract NAS5-20093 from Goddard Space Flight Center and by Grants NGL-16-001-043 and NGL-16-001-002 from NASA Headquarters, and by the Office of Naval Research.

REFERENCES

Benediktov, E. A., G. G. Getmantsev, Yu. A. Sazonoy and A. F. Tarasov, Preliminary results of measurement of the intensity of distributed extraterrestrial radio-frequency emission at 725 and 1525-kHz frequencies by the satellite elektron-2, Kosmicheskie Issledovaniya, 3, 614, 1965.

Benson, R. F., and W. Calvert, Isis I observations at the source of auroral kilometric radiation, Geophys. Res. Lett., 6, 479, 1979.

Brown, L. W., Possible radio emission from Uranus at 0.5 MHz, Astrophys. J., 207, L202, 1976.

Carlqvist, P., and R. Bostrom, Space-charge regions above the aurora, J. Geophys. Res., 75, 7140, 1970.

Chiu, Y. T., and M. Schlulz, Self-consistent particle and parallel electrostatic field distributions in the magnetospheric-ionospheric auroral region, J. Geophys. Res., 83, 629, 1978.

Dunkel, N., B. Ficklin, L. Rorden, and R. A. Helliwell, Low-frequency noise observed in the distant magnetosphere with OGO 1, J. Geophys. Res., 75, 1854, 1970.

Frank, L. A., and K. L. Ackerson, Observations of charged-particle precipitation into the auroral zone, J. Geophys. Res., 76, 3612, 1971.

Green, J. L., D. A. Gurnett, and R. A. Hoffman, A correlation between auroral kilometric radiation and inverted-V electron precipitation, J. Geophys. Res., 84, 5216, 1979.

Gurnett, D. A., The earth as a radio source: Terrestrial kilometric radiation, J. Geophys. Res., 79, 4227, 1974.

Gurnett, D. A., and J. L. Green, On the polarization and origin of auroral kilometric radiation, J. Geophys. Res., 83, 697, 1978.

Gurnett, D. A., R. R. Anderson, F. L. Scarf, R. W. Fredricks, and E. J. Smith, Initial results from the ISEE-1 and -2 plasma wave investigation, Space Sci. Rev., 23, 103, 1979.

Helliwell, R. A., Whistlers and related ionospheric phenomena, Stanford Univ. Press, Stanford, CA, 206, 1965.

Hubbard, R. F., and G. Joyce, Simulation of auroral double layers, J. Geophys. Res., 84, 4297, 1979.

Inan, U. S., T. F. Bell, and R. A. Helliwell, Nonlinear pitch-angle scattering of energetic electrons by coherent VLF waves in the magnetosphere, J. Geophys. Res., 83, 3235, 1978.

Kaiser, M. L., M. D. Desch, J. W. Warwick, and J. B. Pearce, Voyager detection of nonthermal radio emission from Saturn, Science, 209, 1238, 1980.

Kundu, M. R., Solar Radio Astronomy, Interscience, New York, 1965.

Lin, C. S., and R. A. Hoffman, Fluctuations of Inverted-V electron fluxes, J. Geophys. Res., 84, 6547, 1979.

Melrose, D. B., An interpretation of Jupiter's radiation and the terrestrial kilometric radiation as direct amplified gyroemission, Astrophys. J., 207, 651, 1976.

Mizera, P. F., and J. F. Fennell, Signatures of electric fields from high and low altitude particle distributions, Geophys. Res. Lett., 4, 311, 1977.

Voots, G., D. A. Gurnett, and S.-I. Akasofu, Auroral kilometric radiation as an indicator of auroral magnetic disturbances, J. Geophys. Res., 82, 2259, 1977.

Warwick. J. W., Radiophysics of Jupiter, Space Sci. Rev., 6, 841, 1967.

Warwick, J. W., J. B. Pearce, A. C. Riddle, J. K. Alexander, M. D. Desch, M. L. Kaiser, J. R. Thieman, T. D. Carr, S. Gulkis, A. Boischot, C. C. Harvey, B. M. Pedersen, Voyager 1 planetary radio astronomy observations near Jupiter, Science, 204, 995, 1979.

Wu, C. S., and L. C. Lee, A theory of terrestrial kilometric radiation, Astrophys. J., 230, 621, 1979.

FIGURE CAPTIONS

Figure 1 — A representative spectrum of auroral kilometric radiation. Note the upper and lower cutoff frequencies of the spectrum and the occurrence of intervals when the radiation disappears completely.

Figure 2 — Idealized velocity distributions illustrating the loss-cone and beam-type free-energy sources. Cyclotron resonance interactions occur along a circle in velocity space with a center at $v_{\parallel} = c\mathrm{Cos}\theta$ and a radius $v_R = c[\mathrm{Cos}\theta - 2\Delta\omega/\omega_g]^{1/2}$.

Figure 3 — A velocity distribution function obtained by S3-3 in the auroral acceleration region [Mizera and Fennel, 1977]. Note the regions of large positive $\partial F/\partial v_{\perp}$ near the loss cone boundary and large positive $\partial F/\partial v_{\parallel}$ just inside the elliptical electrostatic acceleration boundary.

Figure 4 An ionospheric model illustrating the control of the upper and lower cutoffs of the kilometric radiation by the electron density profile and the electrostatic potential distribution. Instability only occurs if the minimum resonance energy, $W_{\parallel RES}(Min)$, is below the electrostatic potential energy $e\Phi_s$.

Figure 5 The distribution of upper and lower cutoff frequencies for Figure 1, and the corresponding radial distance, assuming that the emission occurs very close to the electron gyrofrequency.

Figure 6 High resolution spectrograms showing the occurrence of many narrowband emissions drifting upward in frequency.

Figure 7 High resolution spectrograms showing the occurrence of many discrete emissions in the auroral kilometric radiation spectrum. These emissions have many features similar to discrete whistler-mode emissions.

Figure 8 The distribution of drift velocities for narrowband drifting features similar to those illustrated in Figure 7.

A-G81-24

DAY 94, APRIL 4, 1978

AURORAL KILOMETRIC RADIATION

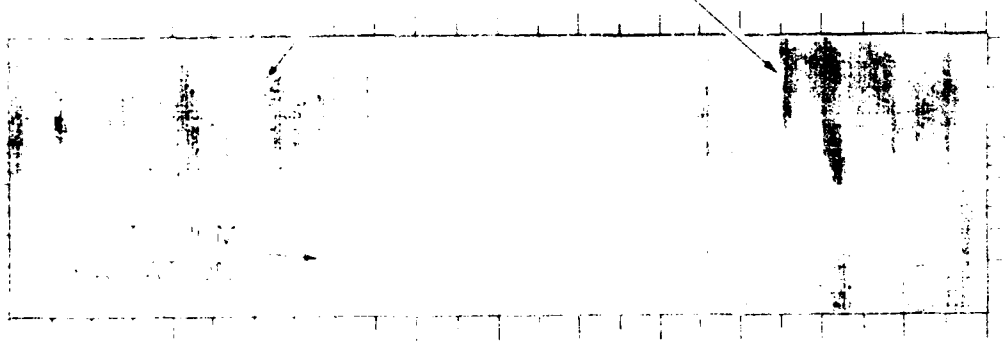

[illegible]	[illegible]	0800	1200	1600	2000	0000
[illegible]	22.3	22.6	22.4	21.6	20.2	18.0
[illegible]	20.6	24.1	11.4	1.8	2.2	10.2
[illegible]	0.	23.9	0.0	0.4	0.8	1.0

Figure 1

C-G81-6

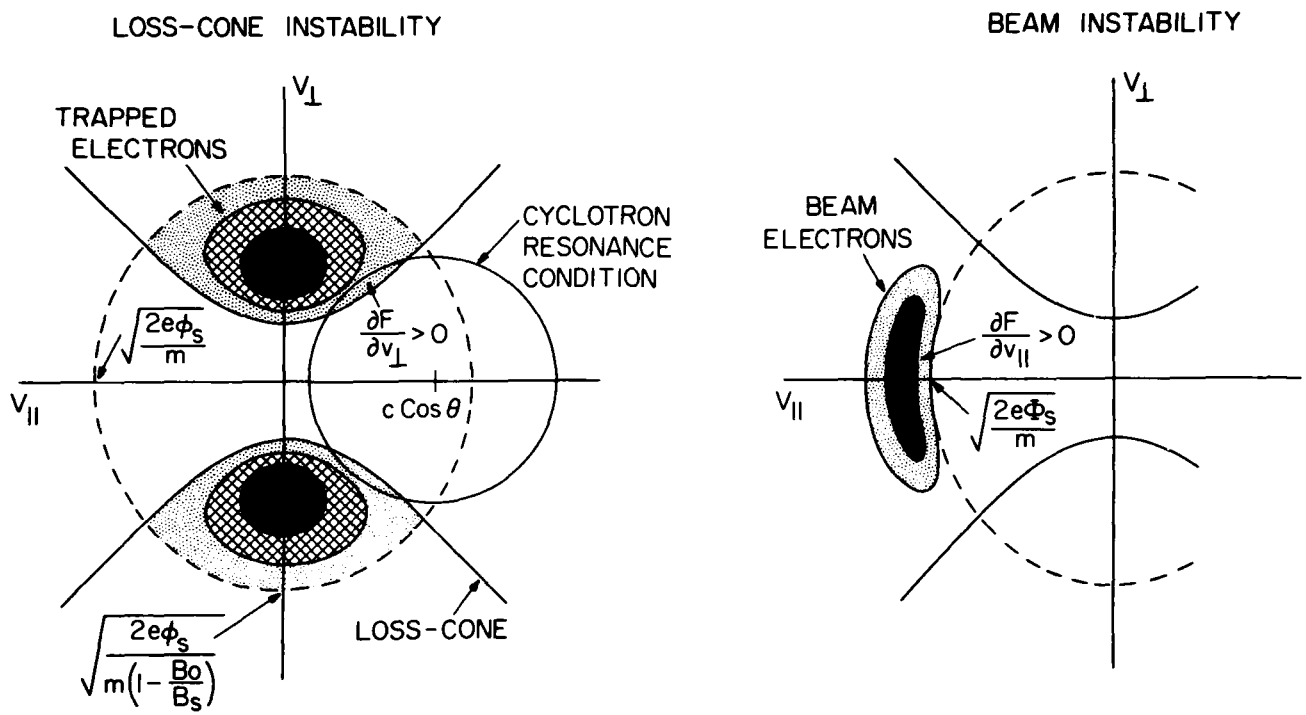

Figure 2

A-G81-41

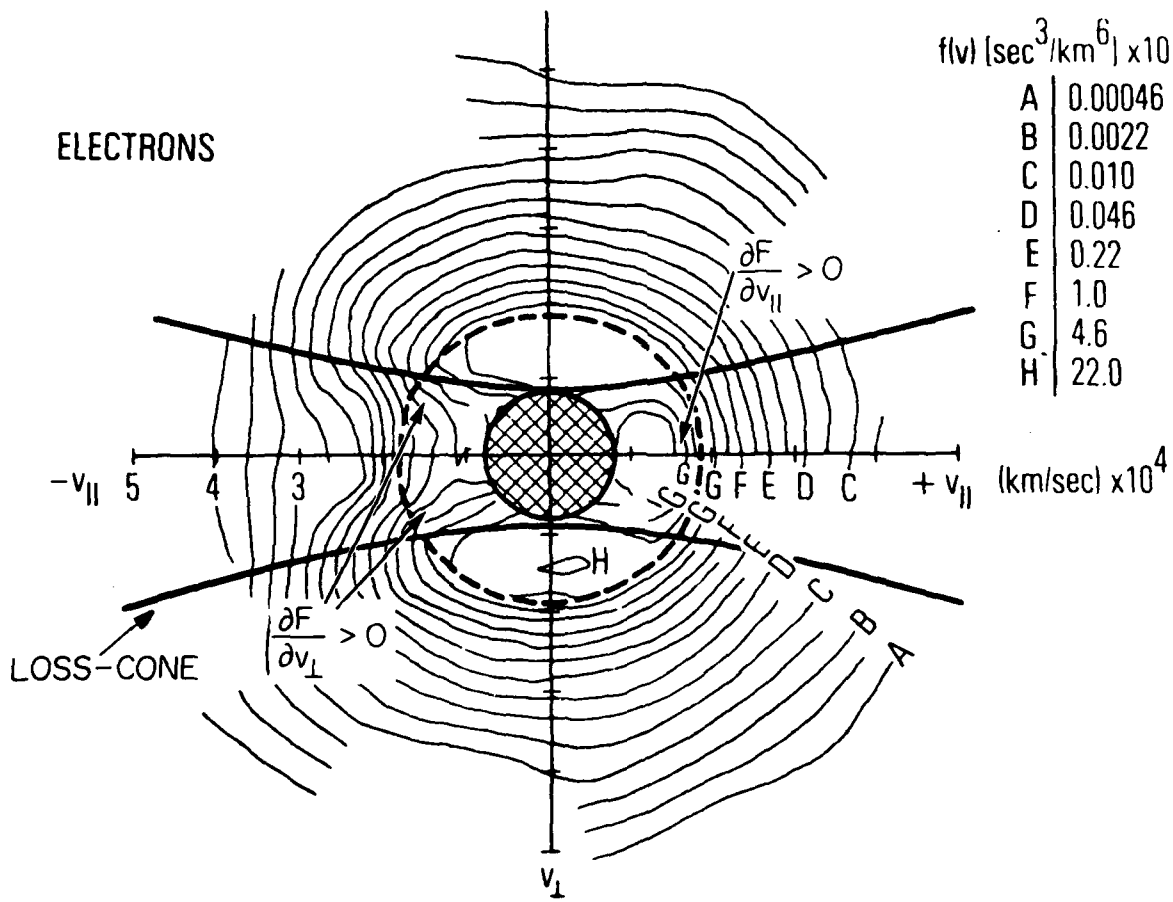

Figure 3

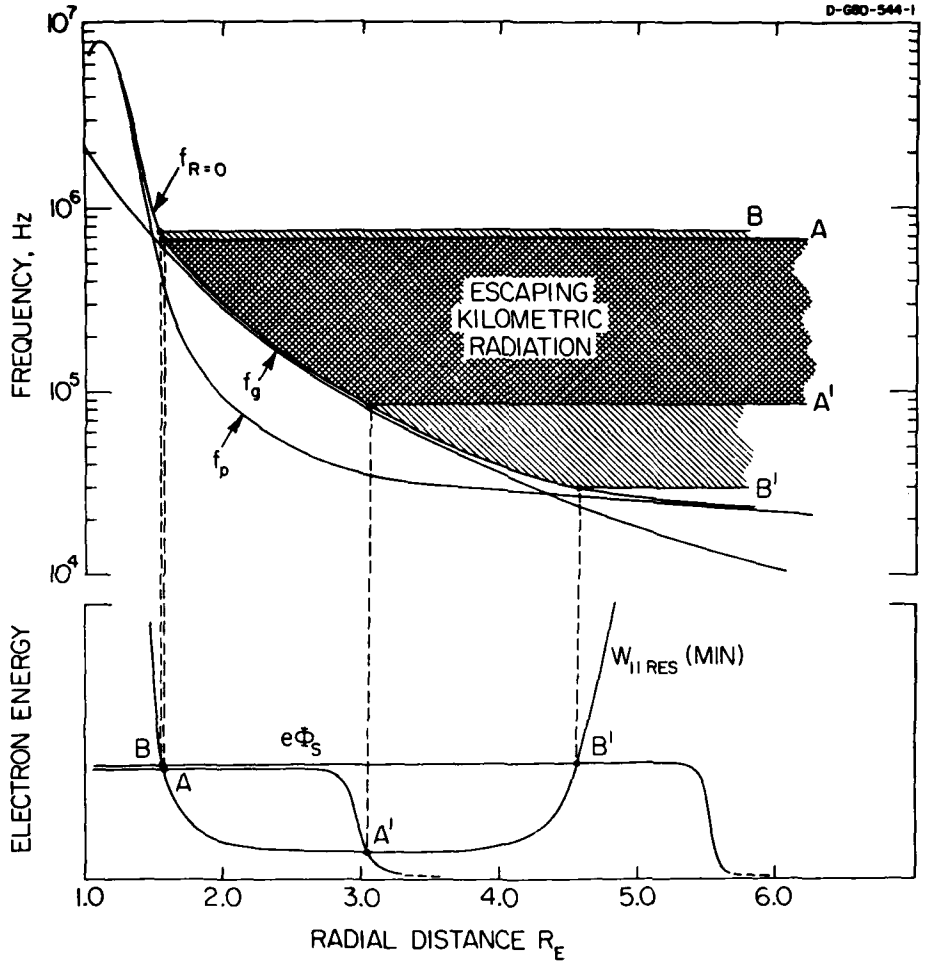
D-GBD-544-1
FREQUENCY, Hz
10^7
10^6
10^5
10^4
$f_{R=0}$
f_g
f_p
B
A
A'
B'
ESCAPING
KILOMETRIC
RADIATION
ELECTRON ENERGY
$W_{\parallel RES}$ (MIN)
$e\Phi_S$
B
A
A'
B'
1.0
2.0
3.0
4.0
5.0
6.0
RADIAL DISTANCE R_E

Figure 4

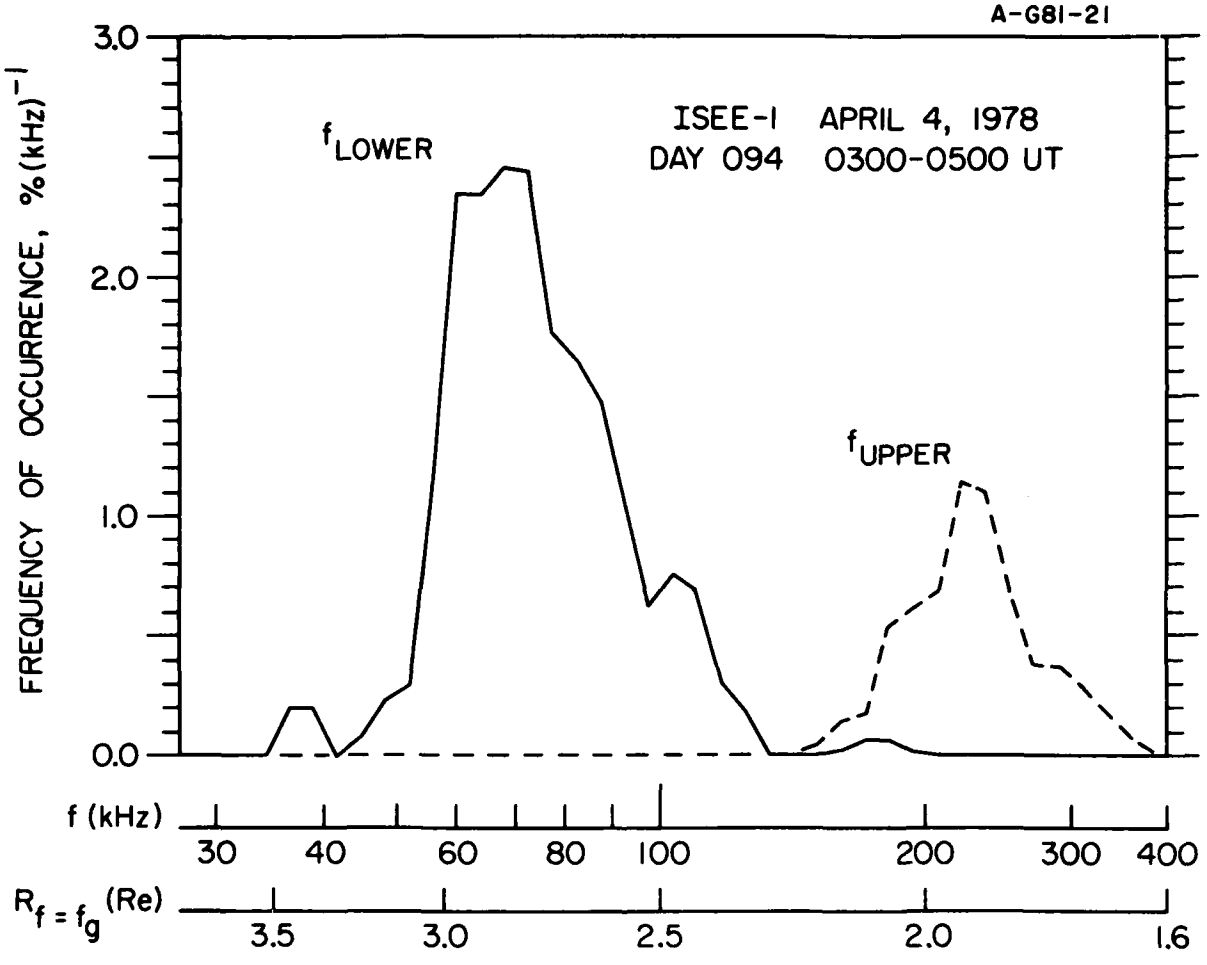
A-G81-21
ISEE-1 APRIL 4, 1978
DAY 094 0300-0500 UT
f_{LOWER}
f_{UPPER}
FREQUENCY OF OCCURRENCE, %(kHz)$^{-1}$
3.0
2.0
1.0
0.0
f (kHz)
30
40
60
80
100
200
300
400
$R_f = f_g$ (Re)
3.5
3.0
2.5
2.0
1.6

Figure 5

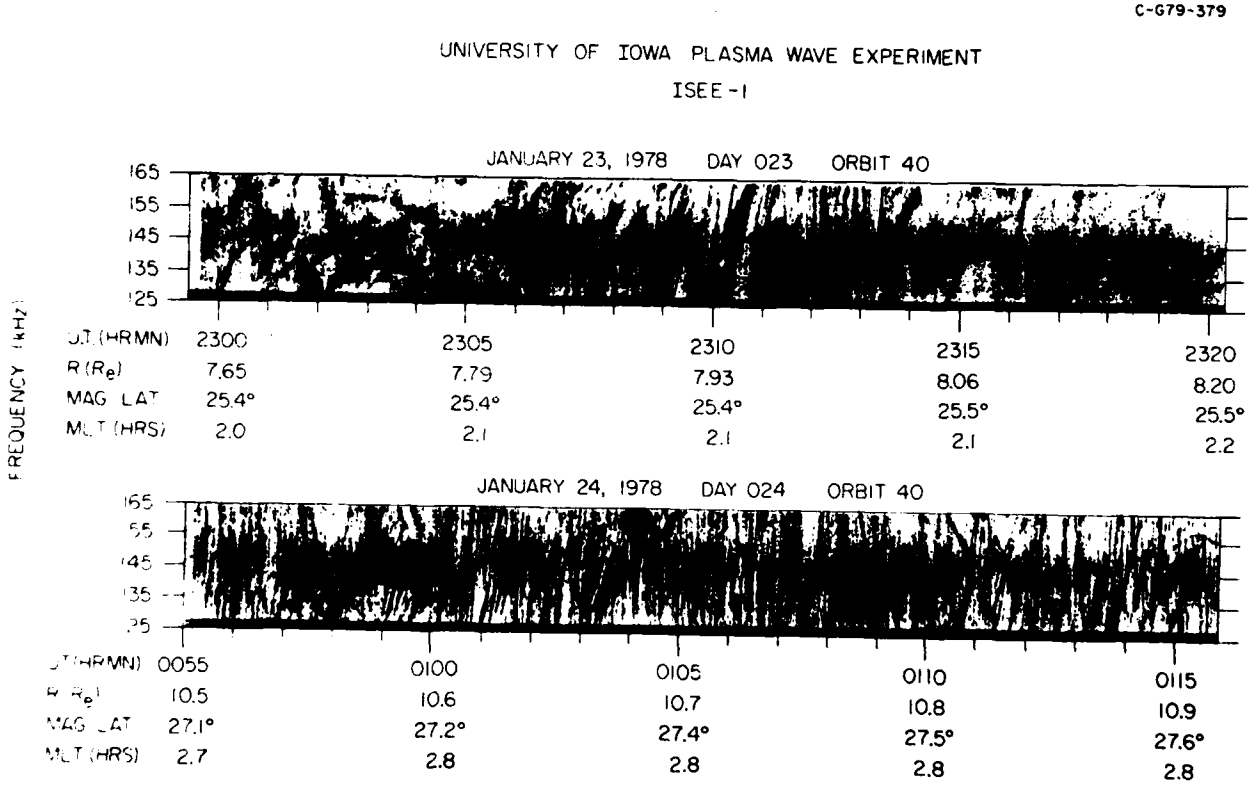
C-G79-379
UNIVERSITY OF IOWA PLASMA WAVE EXPERIMENT
ISEE-1
JANUARY 23, 1978 DAY 023 ORBIT 40
FREQUENCY (kHz)
165
155
145
135
125
U.T.(HRMN) 2300 2305 2310 2315 2320
R(Re) 7.65 7.79 7.93 8.06 8.20
MAG LAT 25.4° 25.4° 25.4° 25.5° 25.5°
MLT (HRS) 2.0 2.1 2.1 2.1 2.2
JANUARY 24, 1978 DAY 024 ORBIT 40
U.T.(HRMN) 0055 0100 0105 0110 0115
R(Re) 10.5 10.6 10.7 10.8 10.9
MAG LAT 27.1° 27.2° 27.4° 27.5° 27.6°
MLT (HRS) 2.7 2.8 2.8 2.8 2.8

Figure 6

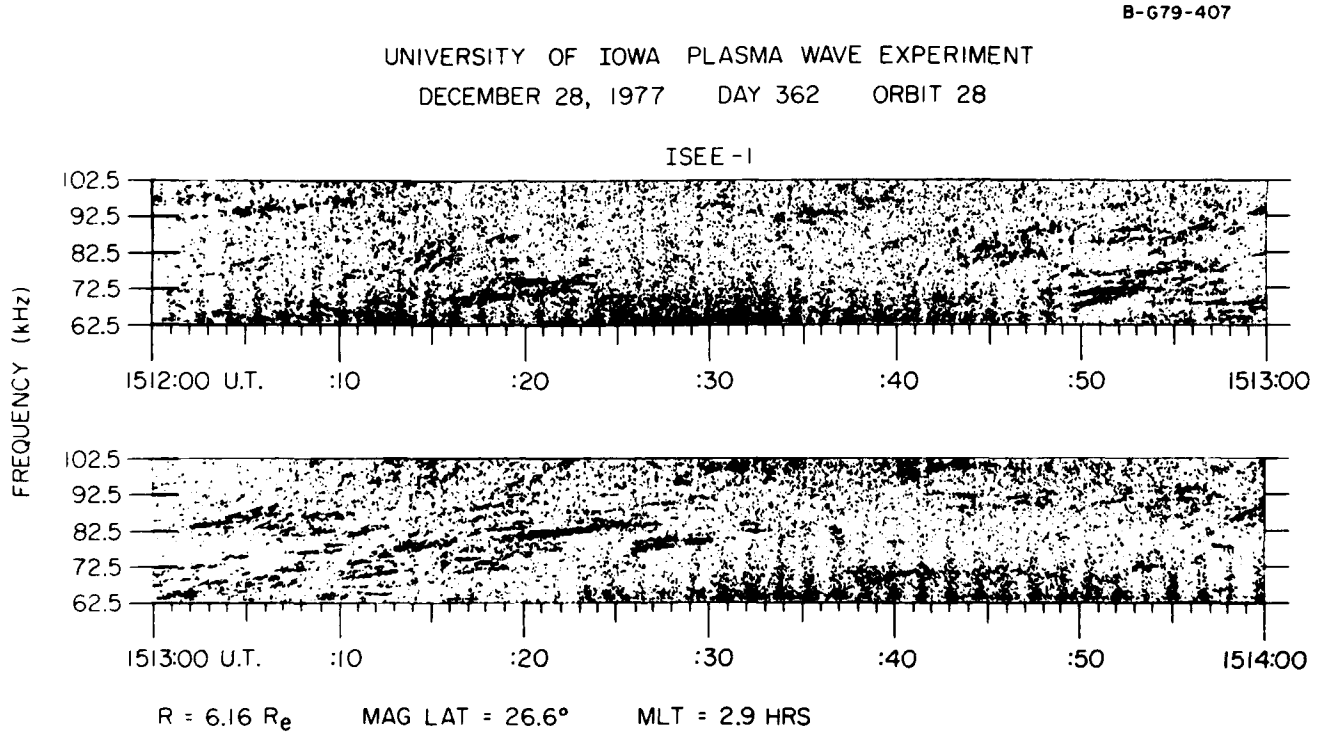
B-G79-407
UNIVERSITY OF IOWA PLASMA WAVE EXPERIMENT
DECEMBER 28, 1977 DAY 362 ORBIT 28
ISEE-1
FREQUENCY (kHz)
102.5
92.5
82.5
72.5
62.5
1512:00 U.T.
:10
:20
:30
:40
:50
1513:00
1513:00 U.T.
1514:00
R = 6.16 R_e
MAG LAT = 26.6°
MLT = 2.9 HRS

Figure 7

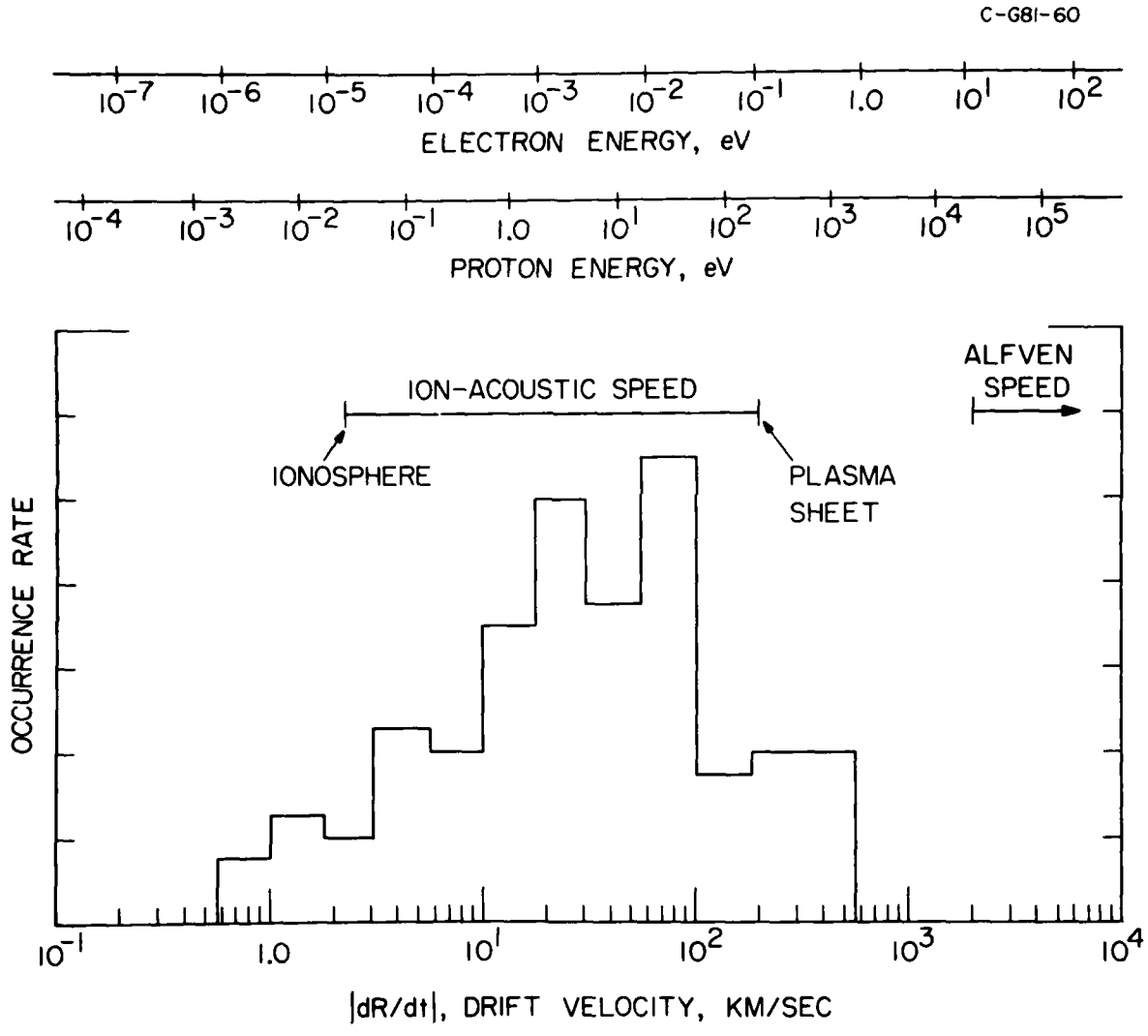
C-G81-60
10^{-7} 10^{-6} 10^{-5} 10^{-4} 10^{-3} 10^{-2} 10^{-1} 1.0 10^{1} 10^{2}
ELECTRON ENERGY, eV
10^{-4} 10^{-3} 10^{-2} 10^{-1} 1.0 10^{1} 10^{2} 10^{3} 10^{4} 10^{5}
PROTON ENERGY, eV
ION-ACOUSTIC SPEED
ALFVEN SPEED
IONOSPHERE
PLASMA SHEET
OCCURRENCE RATE
10^{-1} 1.0 10^{1} 10^{2} 10^{3} 10^{4}
|dR/dt|, DRIFT VELOCITY, KM/SEC

Figure 8